SME Annual Meeting
Feb. 24 - 27, 2018, Denver, CO

Preprint 19-145

SHIELDING MATERIAL COMPARISON FOR ELECTROMAGNETIC INTERFERENCE MITIGATION FOR THE AIR PUMP MOTOR OF PERSONAL DUST MONITORS

J. Li, CDC NIOSH, Pittsburgh, PA
J. Carr, CDC NIOSH, Pittsburgh, PA
C. Zhou, CDC NIOSH, Pittsburgh, PA
C. DeGennaro, CDC NIOSH, Pittsburgh, PA
B. Whisner, CDC NIOSH, Pittsburgh, PA
P. McElhinney, CDC NIOSH, Pittsburgh, PA

ABSTRACT

Since 2016, electromagnetic interference (EMI) of personal dust monitors (PDMs) with magnetic proximity detection systems (PDSs) has been observed in underground coal mines. The EMI causes the magnetic field measurements of a PDS to change, which, in turn, alters the calculated location of the miner relative to the machine. The search for EMI mitigation strategies led to the development and use of large shielding pouches and boxes to hold the entire PDM to reduce its magnetic emission. Research on these pouches and boxes found that although they were able to reduce the emitted radiation from the PDM, they also disturbed the magnetic field of the PDS, affecting its performance. Researchers from the National Institute for Occupational Safety and Health (NIOSH) have focused on shielding internal PDM components rather than shielding the entire PDM. The PDM air pump motor is one of the PDM components that has been identified as a major source of electromagnetic radiation and has been selected for further study and tests. The measurements show that a small copper or aluminum foil enclosure can effectively reduce the magnetic emission of the motor by between 50% and 85% at 73 kHz. This study compares the test results of the air pump motor with various shielding materials.

INTRODUCTION

Work in underground coal mines presents a number of uniquely difficult safety and health challenges. Among the health hazards is the risk of respiratory diseases due to dust exposure. To address this hazard, the Mine Safety and Health Administration (MSHA) mandates the use of a continuous personal dust monitor (CPDM), a battery-powered device that the miner wears on his or her belt to take continuous dust samples for designated occupations and designated areas (30 CFR § 70).

Among the safety hazards in an underground coal mine is the risk that a miner may become struck or pinned by a piece of mobile machinery such as a continuous mining machine or other mobile equipment. To address this hazard, MSHA requires that all continuous mining machines, except full-face machines, must be equipped with a proximity detection system (PDS) (30 CFR § 75.1732). A PDS consists of machine-mounted and miner-wearable components that communicate with low frequency signals to determine the position of the miner relative to the machine and to issue warnings or automatically disable machine motion in order to prevent the machine from contacting the miner. The miner-wearable component of the PDS is typically worn by the miner on his or her belt. Since the PDM is also worn on the miner's belt, these two devices can be placed near each other.

Incidents of electromagnetic interference (EMI) of one model of CPDM, which we will refer to as the PDM, with the PDS in underground coal mines have been reported, and NIOSH researchers have verified through laboratory experiments that EMI is occurring. The EMI affects the readings of the PDS in such a way that the calculated location of the miner becomes unreliable. This creates a serious safety concern since it can effectively render the PDS non-operational during the EMI incident.

In an effort to mitigate the effects of this EMI, large shielding pouches and boxes were developed to enclose the entire PDM to reduce its magnetic emission. Research showed that the pouches and boxes reduced the emitted radiation, but they also disturbed the magnetic field, affecting the performance of the PDS (Noll et al., 2017; Noll et al., 2018a; Noll et al., 2018b).

In order to find a better solution, researchers from the NIOSH have turned their focus from external shielding of the entire PDM to internal shielding of individual PDM components. The research team identified the PDM air pump motor as one of the major sources of electromagnetic radiation within the PDM and selected this pump assembly for further tests. The research team conducted a series of tests on this pump and showed that a copper or aluminum foil enclosure can effectively reduce the magnetic emission from the motor by between 50% and 85% at 73 kHz, which is the operating frequency of one MSHA-approved PDS used in underground mines. With this shielding around the pump motor, the magnetic emission of the motor is reduced to well below the susceptibility threshold at which it could interfere with the PDS. While this result is promising, it should be noted that the air pump motor is only one of several components within the PDM that may cause EMI. An investigation of the other components within the PDM is currently underway. This study compares the shielding effects of copper, aluminum, and other materials that could be used to shield the motor. The information provided in this paper can be used by PDM and other electronic device manufacturers to develop an EMI shielding strategy for internal device components; this could make mines safer by mitigating the problems of EMI and thereby improving the robustness of PDSs.

METHOD AND EXPERIMENTAL SETUP

NIOSH researchers have developed a test method to measure the shielding effectiveness of the enclosures that are particularly applicable to the air pump motor. Some standardized EMI measurement methods, such as RE101, were referenced and adapted in the development of the NIOSH test method (MIL-STD-461F, 2007; Eckert, 1988). In addition, the method of determination of shielding effectiveness was also developed by referencing and adapting some standardized methods (Ott, 2009; Montrose and Nakauchi, 2004). In the experiment, the enclosure was made to directly touch the surface of the air pump motor assembly, which has an irregular shape.

The air pump motor is one of the internal components, powered by a 12-V supply with a mode of pulse-width modulation (PWM). The pulse width changes with changes in measurements from on-board temperature, humidity, and other sensors. To measure emission exclusively from the motor, the motor was removed from the PDM case and provided with a stabilized 12 V pulse supply, varying in frequency. During testing, two diode scubbers remained connected to the motor terminals. A total of 12 pulse frequencies were selected, which included DC, 10 Hz, 20 Hz, 30 Hz, 40 Hz, 50 Hz, 100 Hz, 200 Hz, 500

Hz, 1,000 Hz, 1,500 Hz, and 2,000 Hz. Figure 1 shows the block diagram of the experimental setup. Figure 2 demonstrates the wave form of a pulse supply voltage.

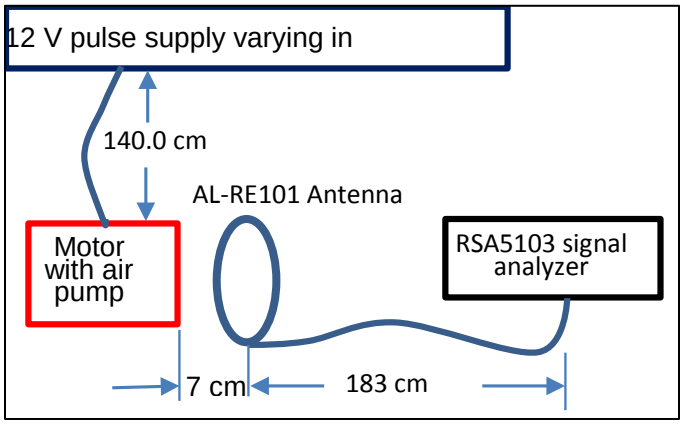

Figure 1. Block diagram of the experimental setup for the PDM air pump motor.

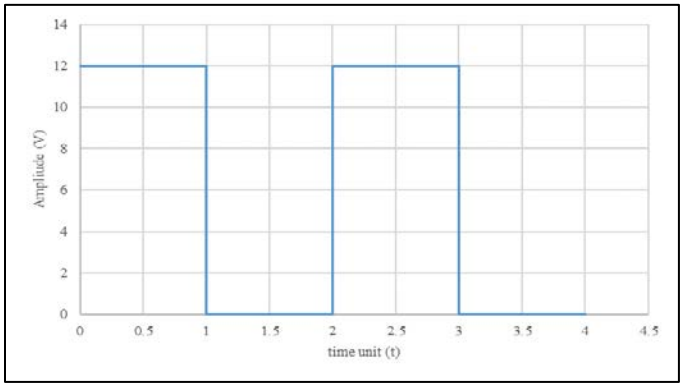

Figure 2. Illustration of pulse supply voltage to the motor.

As shown in Figure 1, the air pump motor was powered by the 12 V pulse supply via a 140.0 cm (55.12 inch) cable. An AL-RE101 antenna was used to measure the magnetic field emission of the motor at a distance of 7 cm (2.76 inches). This is the distance that is used by a standardized RE101 test (MIL-STD-461F, 2007). The antenna feeds the emission measurements from the motor to a Tektronix RSA5103A Real-Time Signal Analyzer via a 183.0 cm (72.0 inch) coaxial cable. The Signal Analyzer stores the raw measurement data in a unit of dBμV. The data were transferred to a computer to convert to magnetic flux density readings in dBpT.

Prior to the emission measurement of the motor, the emission of the pulse power supply unit was measured at a distance of 140.0 cm. These measurements showed that the power supply unit would have a very insignificant influence on the emission measurements of the motor. The measurements also showed that the influence of the signal analyzer to the antenna was very insignificant. Furthermore, the measurements showed that the ambient electromagnetic noise was low.

A GAST 1001126-204-1089 motor model is used in the air pump. Figure 3 shows the air pump motor assembly; the metallic cylinder in the photograph is the electric motor and the black plastic housing attached to the motor contains the air pump. The magnetic field emission measurements were made on six orthogonal sides of the air pump motor assembly. Figure 4 shows a picture of the motor with one side sitting on the test platform with no shielding materials applied. The air pump has a rubber air tube connected with an air filter at the opposite end of the tube.

The AL-RE101 antenna has a usable frequency range of 10 Hz to 1 MHz. In this experiment, the measurements of the emitted magnetic field from the motor were set in a frequency band from 10 kHz to 150 kHz, which covers the operating frequencies used by all of the current commercial PDSs. Any unintended magnetic field emissions from the motor in this frequency band that could cause an interference with the proximity detection systems can then be identified.

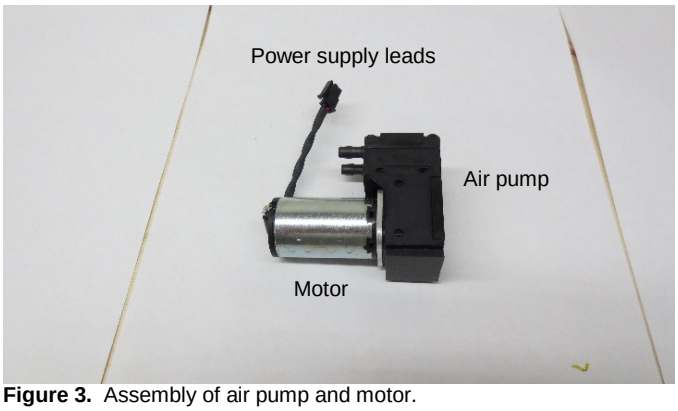

Figure 3. Assembly of air pump and motor.

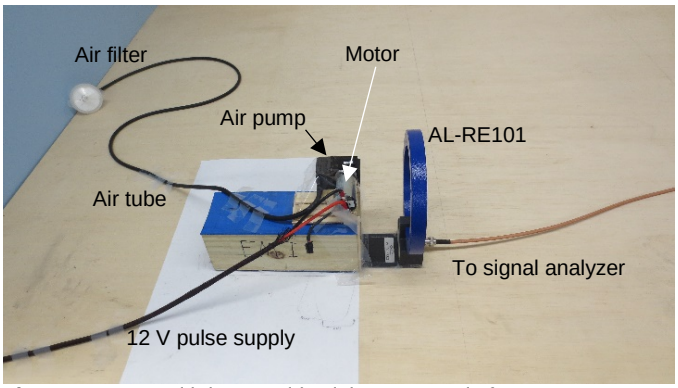

Figure 4. Motor with its one side sitting on test platform.

TEST RESULTS

The magnetic field emission measurement on the motor began with no shielding material applied. The emissions from the six sides of the motor were measured individually and used as the baseline of the motor emission. The baseline emission measurement from each side was later compared to the emission measurement of the corresponding side of the motor with different shielding materials applied. The shielding effect of each of the materials was then identified. The shielding materials and their thicknesses used in the experiment were: aluminum foil of 0.0254 mm (0.001 inches), aluminum foil of 0.0508 mm (0.002 inches), copper foil of 0.016256 mm (0.00064 inches), copper mesh of 0.1143 mm (0.0045 inches) diameter wire and 0.1397 mm (0.0055 inches) opening, graphene sheet of 0.254 mm (0.01 inch), stainless steel mesh of 0.09906 mm (0.0039 inches) diameter wire and 0.09906 mm (0.0039 inches) opening, and silver-graphene epoxy.

Figure 5 shows the magnetic field emission measurements from side 3 of the motor with no shielding material applied, referring to Figure 4 for the experimental setup. In addition to the emission spectra, from 10 kHz to 150 kHz, of the motor with 12 supply voltages in different pulse frequencies, a susceptibility curve of a PDS measured in NIOSH's previous research (Noll et al., 2017) is also given in the figure for the purpose of identification of potential EMI from the motor emission. Any portion of an emission curve of the motor crossing and reaching above the susceptibility curve suggests that there is a high potential for interference to occur because of the stronger energy of the emitted magnetic field of the motor compared to the susceptibility of the PDS. The emission curves of the motor produced from the 12 supplied pulse voltages, as shown in Figure 5, have a high potential to cause an interference around 73 kHz because these emission curves all pass above the PDS susceptibility frequency around 73 kHz.

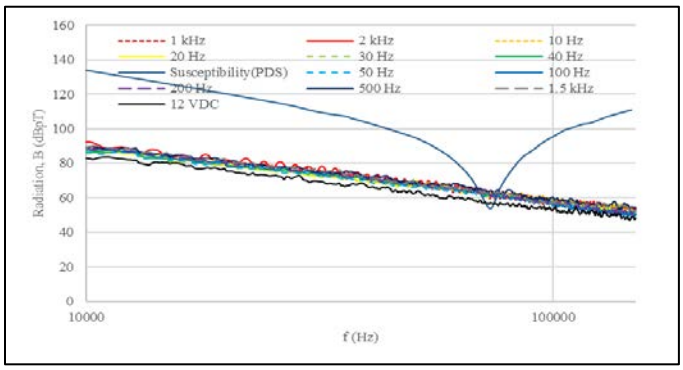

Figure 5. Comparing magnetic field emission from side 3 of the motor having no shielding to the susceptibility of a PDS.

Figure 6 shows the experimental setup for the emitted magnetic field measurement of side 3 of the motor shielded completely with one layer of 0.0508 mm aluminum foil. The shielding layer was tightly wrapped on the motor with the adhesive insulation tape to hold and form an enclosure from outside. The shielding was also extended around the immediate leads of the motor. No electrical ground connection was made between the shielding enclosure and the motor. Figure 7 shows the magnetic field emission measurements from side 3 of the shielded motor. Comparing the emission measurements of the side 3 with the baseline, shown in Figure 5, one could find that the aluminum foil brought all emission curves downward. A calculation from the computer program developed in this study shows that the shielding enclosure attenuates the magnetic energy emission by 71.37% on average at 73 kHz.

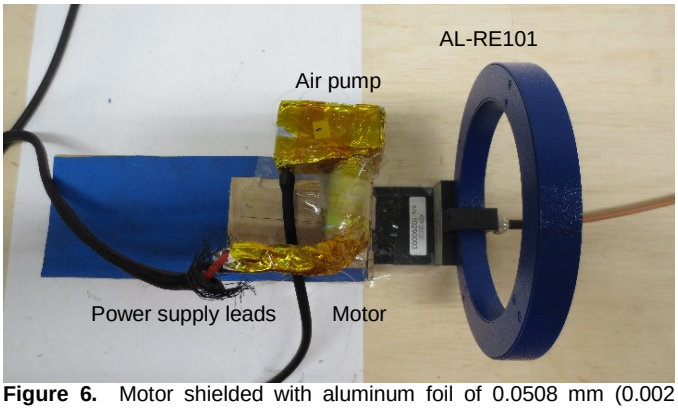

Figure 6. Motor shielded with aluminum foil of 0.0508 mm (0.002 inches) thickness.

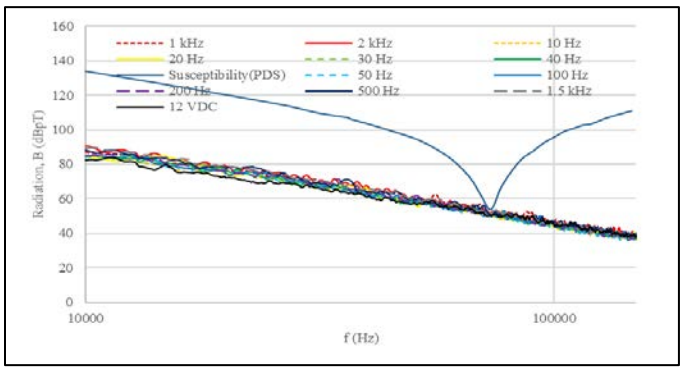

Figure 7. Magnetic field emissions from side 3 of the motor shielded with one layer of aluminum foil of 0.0508 mm or 0.002 inches thickness.

Figure 8 shows the magnetic field emission measurements from side 3 of the motor shielded with one layer of copper mesh with a wire diameter of 0.1143 mm (0.0045 inches) and an opening of 0.1397 mm (0.0055 inches). The motor was shielded in the same manner as that with the aluminum enclosure shown in Figure 6.

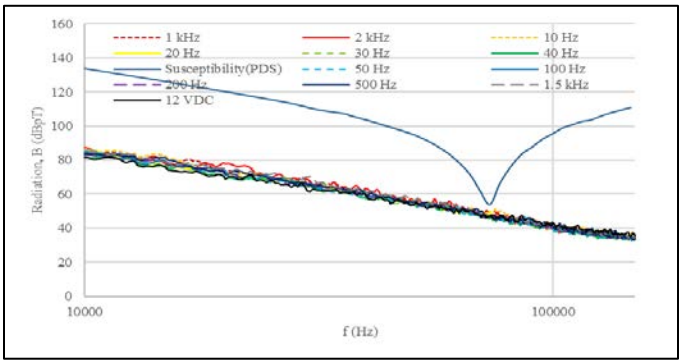

Figure 8. Magnetic field emission from side 3 of the motor shielded with an enclosure of one layer of copper mesh with wire diameter of 0.1143 mm (0.0045 inches) and opening of 0.1397 mm (0.0055 inches).

As shown in Figure 8, all of the emission curves of side 3 of the motor were brought down by the copper mesh enclosure further than the aluminum foil enclosure. As a result, the emission no longer has a potential to interfere with the PDS. A calculation from the computer program developed in this study shows that the copper mesh enclosure attenuates the emission from side 3 of the motor by 84.92% on average at 73 kHz.

With the same shielding manner, we measured the emissions from side 3 of the motor with each of the shielding materials. Figure 9 shows the average emission attenuations of those different shielding materials and material thicknesses at 73 kHz on the emission from side 3 of the motor. In Figure 9, Al .001" stands for aluminum foil with 0.001 inch thickness, Al .002" for aluminum foil with 0.002 inch thickness, Cu .00064 for copper foil with 0.00064 inch thickness, Ag-graphene for silver-graphene epoxy, Cu mesh for copper mesh. Copper and aluminum clearly show a higher shielding effect than the other materials and were more effective with greater thickness.

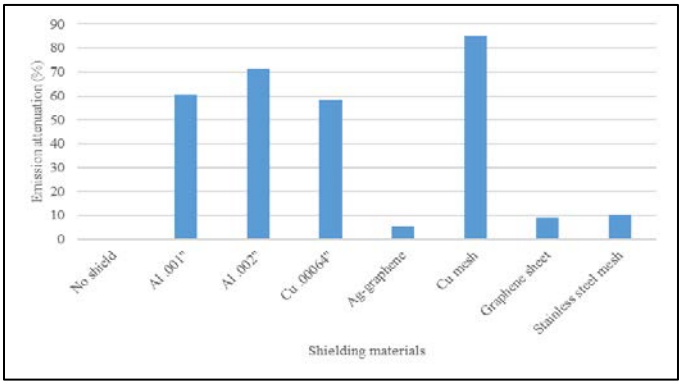

Figure 9. Average emission attenuations on side 3 of the motor with different shielding materials.

The magnetic field emission from each of the sides of the motor was measured in the same manner with each of the shielding materials. The measurements show that the emission attenuations were different from different sides, even with the same shielding material. For example, Figure 10 shows the average emission attenuation of each of the sides of the motor shielded with copper foil at 73 kHz. As it can be seen, the copper foil did not equally attenuate the magnetic emission on all of sides of the motor. Note that the measurements also show that the magnetic field emission strength from each side of the motor with no shielding material applied was also largely different from each other. Side 2 had the lowest no-shielding emission, which also had the lowest emission attenuation as shown in Figure 10.

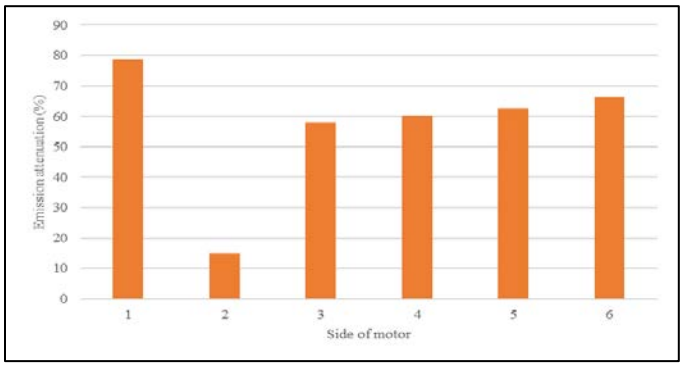

Figure 10. Comparison of the average emission attenuations of six sides of the motor shielded with copper foil of 0.016256 mm (0.00064 inches) thickness at 73 kHz.

Figure 11 shows the average emission attenuations with different shielding materials on all of the sides of the motor at 73 kHz. Similar to side 3, copper and aluminum show a higher effectiveness at attenuating the emission of the motor and more effective with greater thickness. The thicker aluminum enclosure was shown to have a higher attenuation percentage value than the thinner one. The thicker copper enclosure also shows a higher attenuation percentage value than the thinner one.

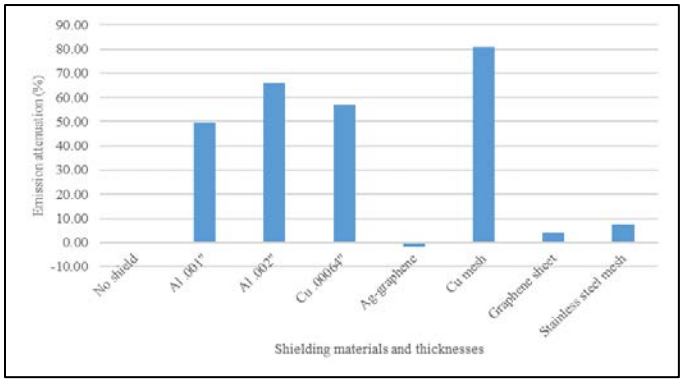

Figure 11. Comparison of the average emission attenuations by the shielding materials and their thicknesses on all of six sides of the motor at 73 kHz.

DISCUSSION

As shown in Figure 11, aluminum and copper show a higher attenuation rate on the emitted magnetic energy of the motor at 73 kHz than any of the other materials tested. The figure also shows that an enclosure with a thicker layer of shielding has a higher emission attenuation rate than that with a thinner one. This suggests that the shielding material and its thickness are important factors to consider for a shielding enclosure design for the motor.

Measurements show that the shielding effectiveness is different from one side of the enclosure to another. This suggests that each of the sides of the enclosure not only shields part of the magnetic energy from that side of the motor, but also reflects part of the energy back, resulting in a redistribution of magnetic energy within the enclosure. This could cause the emission from another side to slightly increase rather than decrease as it showed in the case of silver-graphene epoxy. As shown in Figure 11, a magnetic emission increase from one of the enclosures causes the average emission to increase with silver-graphene. Further study may be needed to understand this phenomenon in order to not only develop better shielding enclosures, but also to prevent the motor's electrical characteristics from potentially being altered by the intensified magnetic energy within the enclosure caused by the shielding enclosures.

A complete coverage over the motor with a shielding enclosure is required in order to achieve a high effectiveness of shielding. Our measurements show that an intensified magnetic energy could be measured from even a small opening on a shielding enclosure. This suggests that the magnetic energy produced from the motor can be redirected by the internal surfaces of the shielding enclosure and released from a small opening of the enclosure. This also suggests that an enclosure can be designed with an opening on it to release the magnetic energy from it in a direction which causes no interference to other systems.

In a separate experiment, we measured the magnetic field emission from the motor with lower DC supply voltages than its normal value of 12 VDC, and found that a lower emission was always associated with a lower voltage. The measurements were not presented in this paper because those lower voltages were not considered to be normal. However, it shows that a supply voltage is indeed a factor that influences the strength of the emitted magnetic field of the motor.

CONCLUSIONS

This paper presents the test results of some selected shielding materials for the air pump motor of a personal dust monitor for the purpose of identifying the effectiveness of these materials on magnetic field shielding for the motor. The measurements show that aluminum and copper can shield the magnetic energy emission of the motor more effectively than any other tested materials. The measurements also show that the thicker a shielding enclosure is, the more effective the shielding. The results provide the measurement data that can lead to the development of effective EMI mitigation strategies for the air pump motor and also for other electronic systems used in underground mines to improve safety for miners.

ACKNOWLEDGMENTS

The authors sincerely thank Mr. Donald Tuchman, Industrial Hygienist of NIOSH, for his support of this work, his comments and data reviewing in the process of this work, and his efforts to provide us with a PDM test unit and other PDM components. The authors also want to express our thanks to Thermo Fisher Scientific for the samples of air pump motor units provided for this work. In addition, we want to thank the Dust Control Branch of the Pittsburgh Mining Research Division of NIOSH for providing support in this work.

Disclaimer

The findings and conclusions in this paper are those of the authors and do not necessarily represent the official position of the National Institute for Occupational Safety and Health, Centers for Disease Control and Prevention. Mention of any company or product does not constitute endorsement by NIOSH.

REFERENCES

Eckert, J., "Commercial EMC Standards of the United States," Volume 9, Interference Control Technology, Inc. pp.J.9–J.22, 1988.

MIL-STD-461F, pp. 91–94 10, December 2007, https://snebulos.mit.edu/projects/reference/MIL-STD/MIL-STD-461F.pdf.

Montrose, M and Nakauchi, E., "Testing for EMC Compliance Approaches and Techniques," IEEE Press, Wiley-Interscience, John Wiley & Sons, Inc., pp. 330–333, 2004.

Noll, J.; Matetic, RJ., Li, J.; Zhou, C.; DuCarme, J.; Reyes, M.; Srednicki, J., "Electromagnetic Interference with Proximity Detection Systems," published in proceedings of Annual Conference of Society of Mining, Metallurgy and Exploration, Denver CO, Feb 19–22. 2017.

Noll, J., Li, J., DeGennaro, C., Zhou, C., Srednicki, J., "Evaluation of Different Shielding Materials for Reducing Electromagnetic Interference of the Personal Dust Monitor", published in proceedings of Annual Conference of Society of Mining, Metallurgy and Exploration, Minneapolis MN, Feb 25 – 28, 2018 A.

Noll, J., Matetic, R. J, Li, J., Zhou, C., DuCarme, J., Reyes, M., Srednicki, J., “Electromagnetic Interference from Personal dust Monitors and Other Electronic Devices with Proximity Detection Systems”, Peered-reviewed Journal of Mining Engineering, Vol. 70, No. 5, pp. 61–68, May 2018 B.

Ott, H., “Electromagnetic Compatibility Engineering,” John Wiley & Sons, Inc., Hoboken, NJ, pp. 238–245, 2009.